Trans Indian Inst Met (2021) 74(12):2991–2999
https://doi.org/10.1007/s12666-021-02362-y

ORIGINAL ARTICLE

Effect of Co-Addition of Ag and Cu on Mechanical Properties of Sn–5Sb Lead-Free Solder

Biao Yuan[1] · Zhimin Liang[2] · Zongyuan Yang[2] · Fei Shen[2] · Da Xu[1] · Liwei Wang[2] · Shaowei Wei[1] · Dianlong Wang[2]

Received: 12 April 2021 / Accepted: 5 July 2021 / Published online: 7 August 2021

Abstract Sn–Sb lead-free solders are considered to substitute the tin–lead solders due to their great mechanical properties. At room temperature, the mechanical properties of Ni/Au/Sn–5Sb/Au/Ni and Ni/Au/Sn–5Sb–0.3Ag–0.05Cu/Au/Ni linear solder joints were investigated by nanoindentation experiments at different loads. The results showed that the Sn–Sb intermetallic compound (IMC) was distributed in the β-Sn matrix in Ni/Au/Sn–5Sb/Au/Ni solder joints. Co-addition of Cu and Ag resulted in the formation of the rod-shaped Cu_6Sn_5 and the fine granular Ag_3Sn IMCs. At the same load and loading/unloading rate, the indentation depth and residual indentation morphologies of Ni/Au/Sn–5Sb–0.3Ag–0.05Cu/Au/Ni solder joints were smaller than those of Ni/Au/Sn–5Sb/Au/Ni solder joints. The hardness of the two kinds of solder joints decreased with the increase in load, while the Young's modulus was independent of load. In addition, compared to the Ni/Au/Sn–5Sb/Au/Ni solder joints, the hardness, Young's modulus and stress exponents of Ni/Au/Sn–5Sb–0.3Ag–0.05Cu/Au/Ni solder joints achieved an improvement due to the co-addition of Ag and Cu.

Keywords Nanoindentation · Sn–5Sb · Lead-free solder · Microstructure · Mechanical properties

✉ Biao Yuan
3317429101@qq.com

[1] China Electronics Technology Group Corp 13th Research Institute, Shijiazhuang 050061, China

[2] School of Materials Science and Engineering, Hebei University of Science and Technology, Shijiazhuang 050018, China

1 Introduction

With the advantages of good wettability, solderability and suitable price, SnPb solder has been used commonly as brazing material in the field of electronic packaging. However, Pb is an element that causes harm to the human and the environment [1]. Therefore, the use of Pb has been greatly restricted, and the replacement of SnPb solder by lead-free solder is an inevitable trend [2, 3]. With the miniaturization of electronic devices and the densification of packaging, a single solder joint bears more force, electrical and thermal loads in service [4, 5]. Then, the solder joints are more prone to failure and affect the reliability of electronic products. Therefore, it is urgent to find new lead-free solders with great mechanical properties.

At present, the research on the mechanical properties of lead-free solders focuses on Sn–Ag, Sn–Sb, Sb–Bi and Sn–Ag–Cu solders. Among the developed lead-free solders, Sn–Sb solders have attracted much attention due to their great mechanical properties and wettability [6, 7]. The reason for the great mechanical properties of these solders is the solid solution hardening effect of the Sb element [8] and the formation of Sn–Sb intermetallic compound (IMC) [9]. However, when the Sb content in the solder is greater than 10% or more, a large amount of Sn–Sb IMCs will be formed in the β-Sn matrix, resulting in the brittle fracture and the reduction in mechanical properties of the solders. Therefore, due to the high melting point of 245 °C and great comprehensive mechanical properties, Sn–5Sb solder has been gradually applied to the connection of high-temperature resistant components of power modules in fields such as wind power generation, solar energy and electric vehicles. And in order to further improve the mechanical properties of Sn–5Sb solder, the most commonly used method is to add alloying elements to it. Therefore, many

researchers have studied the influence of different alloying elements on the mechanical properties of Sn–5Sb solder. It is found that the appropriate addition of Ag, Au, Bi or Cu elements could improve its mechanical properties to varying degrees, but the strengthening mechanisms of these elements are different. The addition of Ag could generate fine Ag_3Sn particles, which are dispersed in the β-Sn matrix to play the role of dispersion hardening [10, 12, 13]. For Au-addition, the hard $AuSn_4$ will be formed and improve the mechanical properties of Sn–5Sb solder [10]. However, excessive Au will increase the brittleness of the solder to deteriorate its mechanical properties. Bi generally does not react with other elements. It is usually solid-dissolved in the matrix in the form of a simple substance with a strong solid solution hardening effect [11, 12]. The addition of Cu could result in the formation of rod-shaped or petal-like Cu_6Sn_5 particles, and the distribution of Cu_6Sn_5 in matrix is expected to improve the mechanical properties of Sn–5Sb solder [11, 13].

In recent years, nanoindentation experiments have proved to be a more effective method to evaluate the mechanical properties of the micro-area of materials due to the advantages of not being affected by the structure and volume of the materials. This method obtains the continuous load–displacement curve by recording the variations of load and depth of the indenter into the material, and then, the hardness, Young's modulus and stress exponent can be obtained [14–18]. It is extremely advantageous to the small samples, or the samples are made of quite soft materials that are difficult to process. Meanwhile, the different curves can be obtained at different positions of the same sample, which are different from the traditional tensile or compression experiments. At present, many researchers have obtained mechanical parameters information of different solders such as Sn–Ag–Cu [19–22], Sn–3.5Ag [23], Sn–58Bi [24, 25] and Au–20Sn [26] by nanoindentation experiments. However, the mechanical properties of Sn–5Sb solder are mainly studied by traditional tensile or compression experiments with bulk as-cast solder. Thus, Sn–5Sb and Sn–5Sb–0.3Ag–0.05Cu lead-free solders were selected to prepare linear solder joints in this paper. And the nanoindentation experiments were carried out at different loads to test the hardness, Young's modulus and stress exponents of two kinds of solder joints and explore the influence of co-addition of Ag and Cu on mechanical properties of Sn–5Sb solder.

2 Materials and Methods

The lead-free solders used in this study were Sn-5 wt%Sb and Sn-5 wt%Sb-0.3 wt%Ag-0.05 wt%Cu. T2 copper with a size of 500 × 500 × 3000 um was selected as the material to be joined. There is an Electroless Nickel/Immersion Gold (ENIG) layer on the actual PCB substrates. Therefore, an ENIG layer was plated on the surface of the copper to make the interface reaction of the copper after reflow and the interface reaction of the Cu pad of the PCB after reflow as consistent as possible. The two square end faces of the two copper bars were reserved for smeared solders at 200 um intervals and then were placed into the SMT nitrogen reflow soldering furnace for soldering. The peak soldering temperature was set at 265 °C. Figure 1 shows the schematic diagram of the linear solder joint. The samples were polished with sandpaper of different meshes and 0.05 um diamond profiler. A solution of 5 ml HCl, 2 g $FeCl_3$, 30 ml H_2O and 60 ml 95% ethanol was used to etch the sample. X-ray diffractometry (XRD), scanning electron microscope (SEM) and energy-dispersive X-ray spectroscope (EDS) tests were used to determine the phases of the selected samples.

In order to evaluate the mechanical properties of Ni/Au/Sn–5Sb/Au/Ni and Ni/Au/Sn–5Sb–0.3Ag–0.05Cu/Au/Ni linear solder joints, all samples were tested on KLA Nano Indenter G200 with a 115° Berkovich indenter at room temperature. The maximum loads of this experiment were 25 mN, 50 mN, 100 mN and 200 mN, respectively. The one-time loading and unloading mode was adopted, the loading and unloading rate was 5 mN/s, and the dwell time at the peak load was defined as 300 s. For the purpose of avoiding the influence of the stress field of the adjacent indentation, indentation spacing should be more than three times the size of the indentation. Each set of experiment parameters was repeated three times to ensure the accuracy of the experiment results. The SEM test was performed on solder joints to observe the indentation morphology at different maximum loads.

3 Results and Discussion

3.1 Microstructure and Elemental Analysis

In order to determine the initial phase, the Ni/Au/Sn–5Sb/Au/Ni and Ni/Au/Sn–5Sb–0.3Ag–0.05Cu/Au/Ni linear

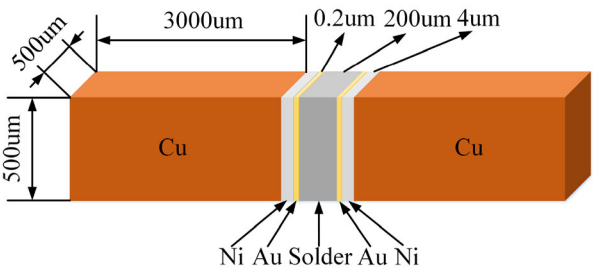

Fig. 1 The schematic diagram of the linear solder joint

solder joints were tested by micro-XRD, and the micro-XRD patterns are shown in Fig. 2a, b. As can be seen from Fig. 2a, the Ni/Au/Sn–5Sb/Au/Ni solder joints are mainly composed of β-Sn and Sn–Sb phase. However, the solder joints containing Ag and Cu exhibit additional IMCs of Ag_3Sn and Cu_6Sn_5, along with the peaks of β-Sn matrix and SbSn phase in all solder joints.

The SEM micrographs of Ni/Au/Sn–5Sb/Au/Ni and Ni/Au/Sn–5Sb–0.3Ag–0.05Cu/Au/Ni solder joints are shown in Fig. 3a, b, and the EDS results of some locations are presented in Table 1. As depicted in Fig. 3a, there are many banded structures in the β-Sn matrix of Ni/Au/Sn-5Sb/Au/Ni solder joints. According to the EDS and micro-XRD results, the banded structures are Sn–Sb phase. In the initial stage of the IMC formation, Sn_3Sb_2 is the first form of Sn–Sb IMC, and then, it decomposes into Sn–Sb solid solution and β-Sn solution at 242 °C according to Sn–Sb equilibrium binary phase diagram [27–30].

In Fig. 3b, the Sn–Sb IMC is also distributed in the β-Sn matrix. However, the morphology of Sn–Sb in Ni/Au/Sn–5Sb–0.3Ag–0.05Cu/Au/Ni is different from Ni/Au/Sn–5Sb/Au/Ni solder joint. Its shape is irregular, such as banded, petal or multilateral. There are some rod-shaped particles and fine granular particles in the Ni/Au/Sn–5Sb–0.3Ag–0.05Cu/Au/Ni solder joint. The EDS and micro-XRD results show that the particles are Cu_6Sn_5 and Ag_3Sn, respectively. The rod-shaped Cu_6Sn_5 in the β-Sn matrix is less because the content of Cu in the solder is only 0.05%. The content of Ag is 0.3% in solder, but Ag has little solubility in the β-Sn matrix. Most of the Ag is precipitated in the form of Ag_3Sn or Ag element during cooling [31]. In this study, only the presence of Ag_3Sn is detected. The Ag_3Sn plays the role of dispersion hardening because the particles are fine and are uniformly distributed in the β-Sn matrix. It is worth noting that EDS results are not accurate with regard to the chemical composition of the phases. The Sn content is overestimated due to the large interaction volume of the electron beam with the Sn matrix which causes the material beneath the particle to emit X-rays. The new Ag_3Sn and Cu_6Sn_5 particles are expected to improve the mechanical properties of Sn–5Sb–0.3Ag–0.05Cu solder.

3.2 Indentation Curves and Indentation Morphology Analysis

The load–displacement (F–h) curves of Ni/Au/Sn–5Sb/Au/Ni and Ni/Au/Sn–5Sb–0.3Ag–0.05Cu/Au/Ni linear solder joints at different loads are plotted in Fig. 4a, b, respectively. As depicted in Fig. 4, the maximum indentation depth increases with the increase in the load from 25 to 200 mN. The stored elastic deformation energy is positively related to the applied load at a constant loading rate. Then, during the stage of holding load, most of the elastic deformation energy is released in the form of creep deformation. This is the reason that a larger load causes a greater indentation depth. The indentation depth information of the two solder joints is listed in Table 2. Apparently, it is seen that at the same load and loading/unloading rate, the maximum indentation depth of the Ni/Au/Sn-5Sb/Au/Ni solder joint is greater than that of Ni/Au/Sn–5Sb–0.3Ag–0.05Cu/Au/Ni solder joint.

The residual indentation morphologies of Ni/Au/Sn–5Sb/Au/Ni and Ni/Au/Sn–5Sb–0.3Ag–0.05Cu/Au/Ni solder joints at 25 mN and 200 mN are shown in Figs. 5a, b and 6a, b, and the values of their residual indentation areas are shown in Table 3. According to Table 3, the size of residual indentation morphology of the Ni/Au/Sn–5Sb/Au/Ni solder joint is bigger than that of Ni/Au/Sn–5Sb–0.3Ag–0.05Cu/Au/Ni. In addition, the slinking-in or piling-up phenomenon is not observed in Figs. 5 and 6. It is considered that there is no significant plastic deformation in the two kinds of solder joints. The smaller the ratio of yield stress and elasticity modulus (σ_y/E) is, the more prone the material is to generate a piling-up phenomenon. And the slinking-in phenomenon generally occurs in materials with large σ_y/E, such as ceramic materials [32]. When the piling-up phenomenon occurs in materials, the position

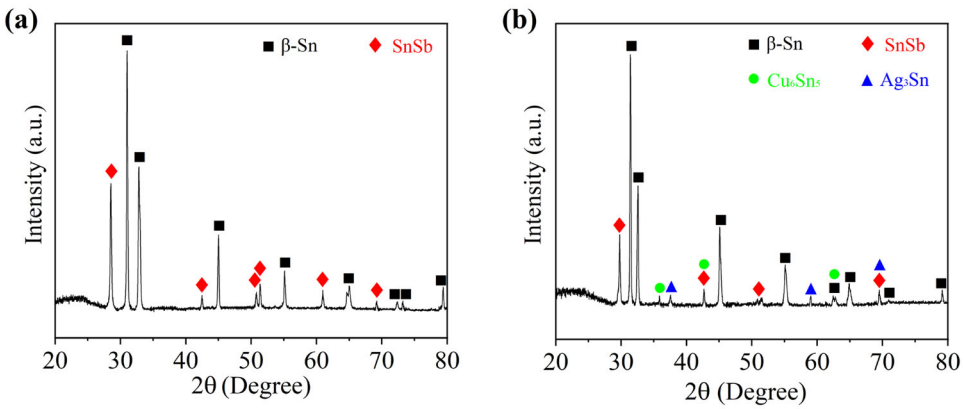

Fig. 2 The micro-XRD patterns for the (**a**) Ni/Au/Sn-5Sb/Au/Ni and (**b**) Ni/Au/Sn–5Sb–0.3Ag–0.05Cu/Au/Ni solder joints

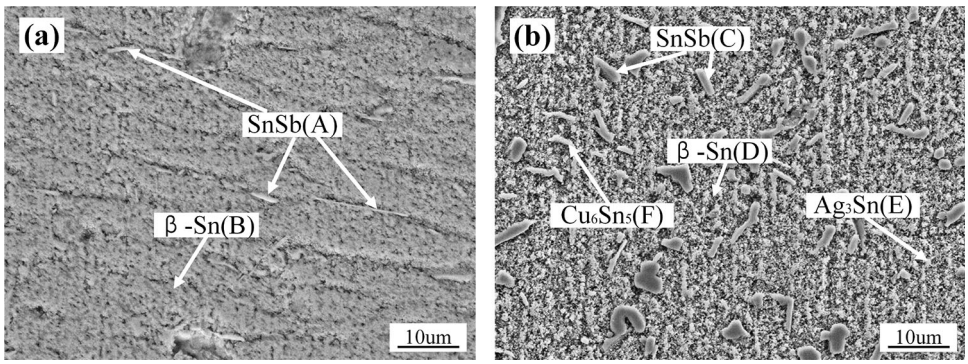

Fig. 3 The SEM micrographs of (**a**) Ni/Au/Sn-5Sb/Au/Ni and (**b**) Ni/Au/Sn–5Sb–0.3Ag–0.05Cu/Au/Ni solder joints

Table 1 Chemical compositions of phases in Ni/Au/Sn–5Sb/Au/Ni and Ni/Au/Sn–5Sb–0.3Ag–0.05Cu/Au/Ni solder joints

Solder joints	Position	Phase	Composition (at%)					
			Sn	Sb	Au	Ni	Ag	Cu
Ni/Au/Sn–5Sb/Au/Ni	A	Sn–Sb	52.9	47.1	–	–	–	–
	B	*β*-Sn	91.2	5.5	1.3	2.0	–	–
	C	Sn–Sb	54.2	45.8	–	–	–	–
Ni/Au/Sn–5Sb–0.3Ag–0.05Cu/Au/Ni	D	*β*-Sn	93.1	6.8	–	0.1	–	–
	E	Ag_3Sn	28.1	0.7	–	–	71.2	–
	F	Cu_6Sn_5	43.6	1.4	–	–	–	55.0

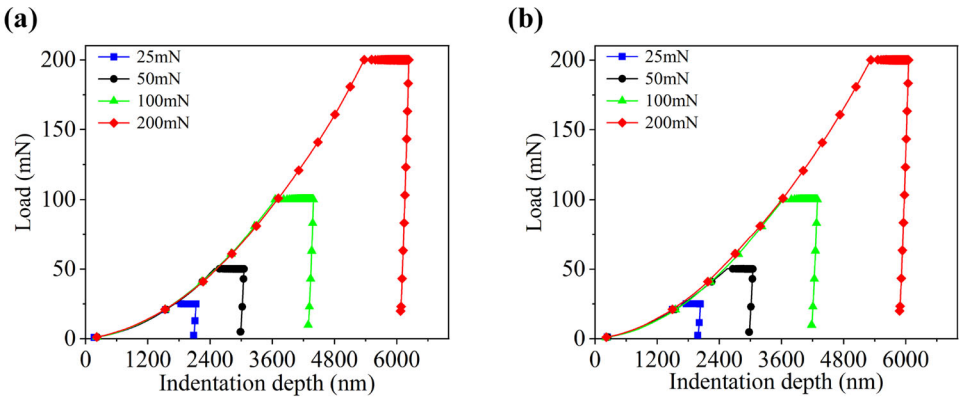

Fig. 4 The load–displacement (*F–h*) curves of (**a**) Ni/Au/Sn-5Sb/Au/Ni and (b) Ni/Au/Sn–5Sb–0.3Ag–0.05Cu/Au/Ni solder joints at different loads

Table 2 The indentation depth of Ni/Au/Sn-5Sb/Au/Ni and Ni/Au/Sn–5Sb–0.3Ag–0.05Cu/Au/Ni solder joints

Solder joints	Maximum indentation depth (nm)				Residual indentation depth (nm)			
	25 mN	50 mN	100 mN	200 mN	25 mN	50 mN	100 mN	200 mN
Ni/Au/Sn-5Sb/Au/Ni	2130	3053	4394	6233	2036	2978	4294	6055
Ni/Au/Sn–5Sb–0.3Ag–0.05Cu/Au/Ni	2083	2985	4293	6073	1985	2920	4182	5881

around the indentation is significantly higher than the initial surface of the material. Then, the actual contact area is bigger than the area calculated by the elastic theory and the hardness value of the material will be overestimated, resulting in the inaccuracy of stress exponent [33]. There is no slinking-in or piling-up phenomenon in this experiment. Therefore, the obtained experimental data can be directly solved for the mechanical parameters without modification.

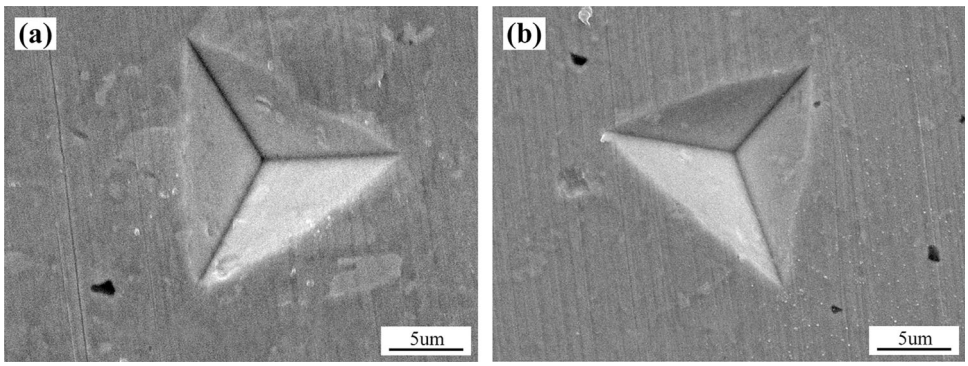

Fig. 5 The residual indentation morphologies of (**a**) Ni/Au/Sn-5Sb/Au/Ni and (**b**) Ni/Au/Sn–5Sb–0.3Ag–0.05Cu/Au/Ni solder joints at 25mN

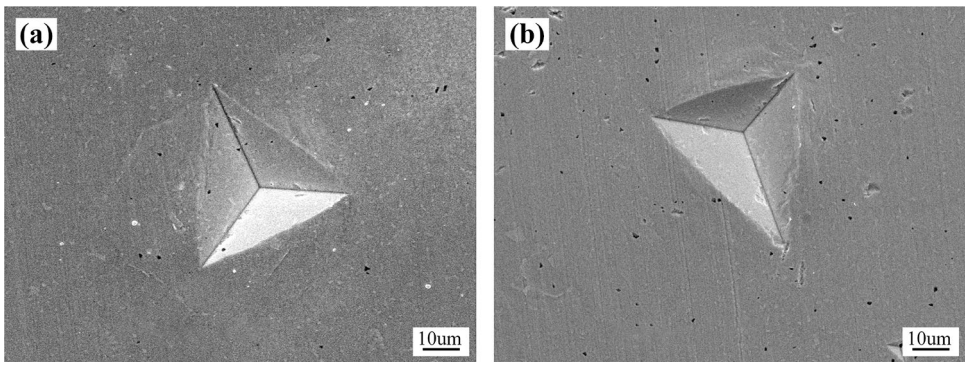

Fig. 6 The residual indentation morphologies of (**a**) Ni/Au/Sn-5Sb/Au/Ni and (**b**) Ni/Au/Sn–5Sb–0.3Ag–0.05Cu/Au/Ni solder joints at 200mN

Table 3 The values of residual indentation areas at 25 mN and 200 mN

Solder joints	Residual indentation areas (um^2)	
	25 mN	200 mN
Ni/Au/Sn–5Sb/Au/Ni	122.83	1032.86
Ni/Au/Sn–5Sb–0.3Ag–0.05Cu/Au/Ni	102.81	940.89

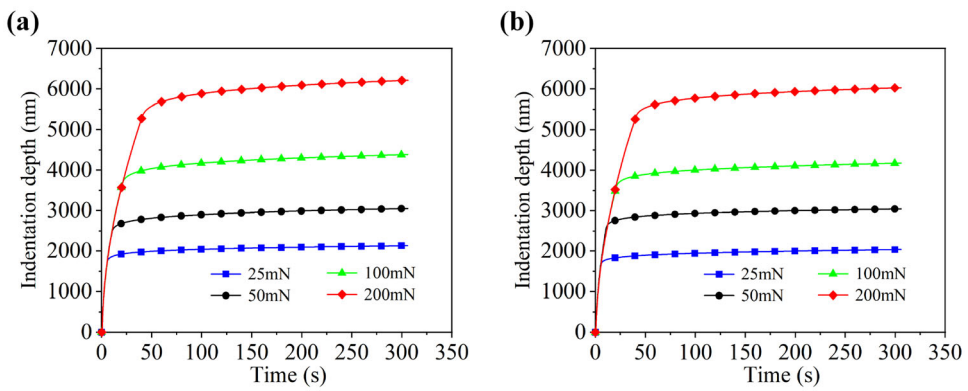

Fig. 7 The displacement–time curves of (**a**) Ni/Au/Sn-5Sb/Au/Ni and (**b**) Ni/Au/Sn–5Sb–0.3Ag–0.05Cu/Au/Ni solder joints at different loads

Figure 7a, b shows the displacement–time curves of Ni/Au/Sn–5Sb/Au/Ni and Ni/Au/Sn–5Sb–0.3Ag–0.05Cu/Au/Ni solder joints at different loads. It can be found that the primary creep stage and secondary creep stage are contained in the curves. The nanoindentation experiment is a compression experiment in nature, and fracture is unlikely to appear in the solder joint. Therefore, the tertiary creep has not been recorded in the displacement–time curves of the nanoindentation experiment that occurs in the ordinary tensile experiment. The creep rate decreases with the

Table 4 Steady-state creep rate of Ni/Au/Sn-5Sb/Au/Ni and Ni/Au/Sn–5Sb–0.3Ag–0.05Cu/Au/Ni solder joints at different loads

Solder joints	Steady-state creep rate (s^{-1})			
	25 mN	50 mN	100 mN	200 mN
Ni/Au/Sn–5Sb/Au/Ni	2.29×10^{-4}	2.39×10^{-4}	2.47×10^{-4}	2.54×10^{-4}
Ni/Au/Sn–5Sb–0.3Ag–0.05Cu/Au/Ni	1.98×10^{-4}	2.05×10^{-4}	2.13×10^{-4}	2.18×10^{-4}

increase in time in the primary creep, followed by the secondary creep in which the creep rate is stable, and indentation depth is considered to increase linearly with the holding time. Table 4 illustrates the steady-state creep rate of Ni/Au/Sn–5Sb/Au/Ni and Ni/Au/Sn–5Sb–0.3Ag–0.05Cu/Au/Ni solder joints at different loads. It can be seen from Table 4 that the steady-state creep rate increases with the increase in load. This is greatly acceptable that bigger loads result in higher steady-state creep rate. At the same loads, the steady-state creep rate of Ni/Au/Sn-5Sb/Au/Ni solder joints is higher than Ni/Au/Sn–5Sb–0.3Ag–0.05Cu/Au/Ni joints. The addition of Ag and Cu leads to the formation Ag_3Sn and Cu_6Sn_5 particles. It is precisely because of the existence of these two particles, and the Ni/Au/Sn–5Sb–0.3Ag–0.05Cu/Au/Ni solder joints have greater creep resistance and lower steady-state creep rate compared to Ni/Au/Sn–5Sb/Au/Ni solder joints.

3.3 Mechanical Properties Analysis

3.3.1 Hardness and Young's Modulus

Figure 8 shows the typical load–displacement curve in the nanoindentation experiment. F_{max} is the maximum load, h_{max} is the maximum indentation depth, h_p is the residual indentation depth, S is the contact stiffness, which is defined as the slope of the top of the unloading curve, and h_r is the intersection of the tangent and the abscissa.

In nanoindentation experiments, the most common method to obtain the hardness and Young's modulus of materials is the Oliver–Pharr method. The hardness H can be defined as:

$$H = \frac{F_{max}}{A_c} \tag{1}$$

where A_c is the projected area of contact between the indenter and the material. For a 115° Berkovich indenter [34]:

$$A_c = 24.56h_c^2 \tag{2}$$

$$h_c = h_{max} - \varepsilon(h_{max} - h_r) \tag{3}$$

where ε is the correction coefficient of the indenter shape, which is related to the geometry of the indenter. In this experiment, $\varepsilon = 0.75$.

The reduced Young's modulus E_r can be expressed as [35]:

$$E_r = \frac{\sqrt{\pi}}{2\beta} \cdot \frac{S}{\sqrt{A_c}} \tag{4}$$

where β is the correction coefficient of the asymmetry of the indenter, for a 115° Berkovich indenter, $\beta = 1.034$.

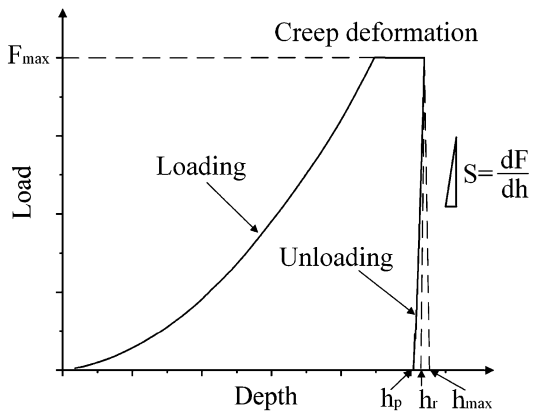

Fig. 8 The typical load–displacement curve in the nanoindentation experiment

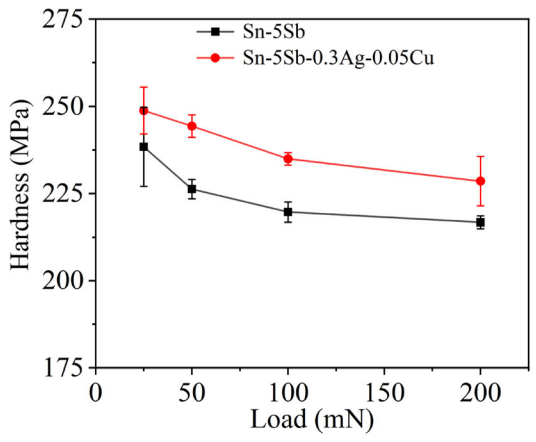

Fig. 9 The hardness of Ni/Au/Sn-5Sb/Au/Ni and Ni/Au/Sn–5Sb–0.3Ag–0.05Cu/Au/Ni solder joints at different loads

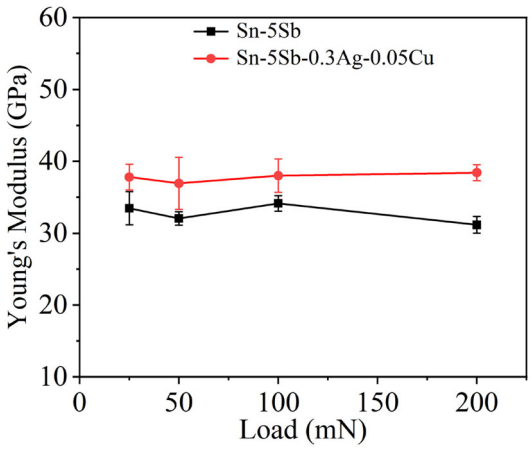

Fig. 10 The Young's modulus of Ni/Au/Sn-5Sb/Au/Ni and Ni/Au/Sn–5Sb–0.3Ag–0.05Cu/Au/Ni solder joints at different loads

The Young's modulus E of the material can be obtained by the following equation [35]:

$$E = \frac{1-\upsilon^2}{1/E_r - (1-\upsilon_i^2)/E_i} \tag{5}$$

where υ and υ_i are the Poisson's ratio of the tested material and the indenter, respectively.

Figures 9 and 10 show the hardness and Young's modulus of Ni/Au/Sn-5Sb/Au/Ni and Ni/Au/Sn–5Sb–0.3Ag–0.05Cu/Au/Ni solder joints at different loads, respectively. It can be seen from Fig. 9 that the hardness values of the two kinds of solder joints decreases with the increase in the load, which indicates that the hardness shows an indentation size effect. In fact, when the indentation depth is less than 50 um or sub-micron in the nanoindentation experiment, the hardness of the material is likely to show a strong indentation size effect; that is, the hardness value has a tendency to decrease with the increase in load. Kong [36] studied the hardness of Cu/SAC305/Cu solder joint at 1–6 mN, and the indentation depth was between 349 and 757 nm. It was found that the hardness decreased with the increase in load because of the indentation size effect. In this experiment, the indentation depth is less than 50 um, so this effect has been observed. As depicted in Fig. 10, the Young's modulus of the two kinds of solder joints is independent of load. In fact, the Young's modulus is an inherent mechanical property parameter of the solder joint, and it is independent of maximum load, holding time, loading/unloading rate and other parameters during the nanoindentation process.

In Figs. 9 and 10, Ni/Au/Sn–5Sb–0.3Ag–0.05Cu/Au/Ni solder joint shows higher hardness and Young's modulus than those of Ni/Au/Sn-5Sb/Au/Ni solder joint. These differences could be related to their microstructure. The co-addition of Ag and Cu generates two smaller-sized Ag_3Sn and Cu_6Sn_5 particles. The Ag_3Sn in the β-Sn matrix has a strong dispersion hardening effect. Therefore, the hardness and Young's modulus of Ni/Au/Sn–5Sb–0.3Ag–0.05Cu/Au/Ni solder joint are higher than those of Ni/Au/Sn-5Sb/Au/Ni solder joint.

3.3.2 Stress Exponent

It is well established that the creep dominates the deformation process when the homogenous temperature (T/T_m, T is the thermodynamic temperature of the service environment of material, and T_m is the thermodynamic temperature of the melting of material) of the material is greater than 0.5 at room temperature. The life of solder is usually determined by the steady-state creep. Hence, most creep constitutive models only consider the creep behavior in the steady-state creep stage. The steady-state creep rate ($\dot{\varepsilon}$) of the solders can be related to the applied stress (σ) by Dorn power law equation [37]:

$$\dot{\varepsilon} = B\sigma^n \exp\left(\frac{-Q}{\mathrm{RT}}\right) \tag{6}$$

where B is the material parameter, n is the stress exponent, Q is the activation energy, R is the universal gas constant, and T is the thermodynamic temperature. Using Eq. (6), the stress exponent could be described as:

$$n = \left(\frac{\partial \ln \dot{\varepsilon}}{\partial \ln \sigma}\right)_T \tag{7}$$

The instantaneous hardness (H) of the material is proportional to applied stress (σ), and the stress exponent can also be expressed by the following equation:

$$n = \left(\frac{\partial \ln \dot{\varepsilon}}{\partial \ln H}\right)_T \tag{8}$$

The deformation of polycrystalline materials with a homologous temperature greater than 0.5 has different creep mechanisms, and the stress exponent is often used to determine the mechanism. However, it should be noted that it is not sufficient to determine the creep mechanism only by comparing the information of the stress exponent. The stress exponent can only be used to narrow the range of possible creep mechanisms. According to recent research, the grain boundary sliding will result in the stress exponent close to 2 [38], the dislocation climb is associated with n values at 4–6 range [39], and the dislocation creep is responsible for $n > 6$.

The creep rate–hardness curves of Ni/Au/Sn-5Sb/Au/Ni and Ni/Au/Sn–5Sb–0.3Ag–0.05Cu/Au/Ni solder joints at different loads are potted in Fig. 11a, b. As depicted in Fig. 11, the stress exponents of Ni/Au/Sn-5Sb/Au/Ni and Ni/Au/Sn–5Sb–0.3Ag–0.05Cu/Au/Ni solder joints at

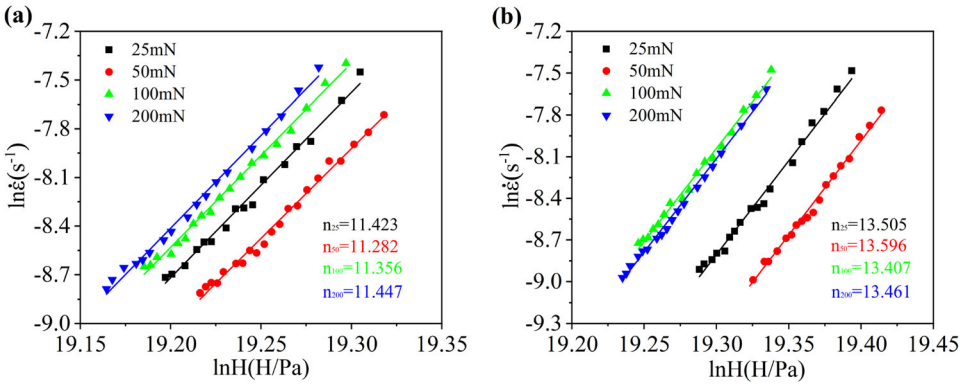

Fig. 11 The creep rate–hardness curves of (**a**) Ni/Au/Sn-5Sb/Au/Ni and (**b**) Ni/Au/Sn–5Sb–0.3Ag–0.05Cu/Au/Ni solder joints

different loads are between 11.282 and 11.447 and 13.407 and 13.596, and the average values are 11.377 and 13.492, respectively. The average stress exponents of the latter are increased by about 18.6% because of the co-addition of Cu and Ag. The fluctuation of the stress exponents may be due to the environmental noise or the accuracy of the instrument. In the present published works, the stress exponents of Sn–5Sb solder are characterized by about 5.4 at the low stress levels [7] and about 11.6 at the high stress levels [40]. It is clear that the stress exponent obtained in this study is equivalent to that at high stress levels.

The difference in creep properties can be attributed to their microstructures of solder joints. In the Ni/Au/Sn–5Sb–0.3Ag–0.05Cu/Au/Ni solder joint, there are many finer Cu_6Sn_5 and Ag_3Sn particles distributed in the β-Sn matrix. It is generally accepted that the interaction between dislocations and particles can result in higher creep resistance in nanoindentation experiments. The particles in Ni/Au/Sn–5Sb–0.3Ag–0.05Cu/Au/Ni solder joint have a more effective blocking effect on dislocation movement because of the formation of Cu_6Sn_5 and Ag_3Sn particles.

4 Conclusions

The microstructures and mechanical properties of Ni/Au/Sn–5Sb/Au/Ni and Ni/Au/Sn–5Sb–0.3Ag–0.05Cu/Au/Ni linear solder joints are studied at room temperature. The following conclusions can be drawn:

(1) The banded Sn–Sb IMC was uniformly distributed in the β-Sn matrix of the Ni/Au/Sn–5Sb/Au/Ni solder joint. Co-addition of Ag and Cu resulted in the formation of dispersed Ag_3Sn and rod-shaped Cu_6Sn_5 particles in the β-Sn matrix.

(2) The indentation depth and residual indentation morphology of Ni/Au/Sn-5Sb/Au/Ni linear solder joint were larger than those of Ni/Au/Sn–5Sb–0.3Ag–0.05Cu/Au/Ni solder joint, indicating that the deformation resistance of the latter was higher than the former. Moreover, there was no slinking-in and piling-up phenomenon in the residual indentation morphology of the two kinds of solder joints. No significant plastic deformation was considered.

(3) The hardness of the two kinds of solder joints decreased with the increase in the load, while the Young's modulus was independent of load. In addition, compared to Ni/Au/Sn–5Sb/Au/Ni solder joint, the Ni/Au/Sn–5Sb–0.3Ag–0.05Cu/Au/Ni solder joint had higher hardness, Young's modulus and stress exponents. This demonstrates that the co-addition of Ag and Cu could improve the mechanical properties of Ni/Au/Sn–5Sb/Au/Ni solder joints.

Acknowledgements This work was supported by Hebei Provincial Key Research Projects (Grant No. 19250202D), National Natural Science Foundation of China (Grant No. 51875168) and Natural Science Foundation of Hebei Province (Grant No. E2020208089/E2019208089/E2020208083).

References

[1] 1. Abtew M, and Selvaduray G, *Mater Sci Eng R Rep* **27** (2000) 95.

[2] 2. Geranmayeh A R, and Mahmudi R, *J Electron Mater* **34** (2005) 1002.

[3] 3. Geranmayeh A R, and Mahmudi R, *J Mater Sci* **40** (2005) 3361.
[4] 4. De Monlevade E F, and Peng W Q, *J Electron Mater* **36** (2007) 783.
[5] 5. Zhu Z, Chan Y C, and Wu F S, *Microelectron Reliab* **92** (2019) 12.
[6] 6. Mahmudi R, Geranmayeh A R, Bakherad M, and Allami M, *Mater Sci Eng A* **457** (2007) 173.
[7] 7. Mahmudi R, Geranmayeh A R, and Rezaee-Bazzaz A, *Mater Sci Eng A* ***448*** (2007) 287.
[8] 8. Murty K L, Haggag F M, and Mahidhara R K, *J Electron Mater* **26** (1997) 839.
[9] 9. McCabe R J, and Fine M E, *Metall Mater Trans A Phys Metall Mater Sci* **33A** (2002) 1531.
[10] 10. El-Daly A A, Swilem Y, and Hammad A E, *J Alloys Compd* **471** (2009) 98.
[11] 11. Esfandyarpour M J, and Mahmudi R, *Mater Sci Eng A* **530** (2011) 402.
[12] 12. Geranmayeh A R, Nayyeri G, and Mahmudi R, *Mater Sci Eng A* **547** (2012) 110.
[13] 13. El-Daly A A, Mohamad A Z, Fawzy A, and El-Taher A M, *Mater Sci Eng A* **528** (2011) 1055.
[14] 14. Esqué-de los Ojos D, Zhang J, Fornell J, Pellicer E, and Sort J, *Mech Mater* **100** (2016) 167.
[15] 15. Nguyen V L, Kim S H, Jeong J W, Lim T S, Yang D Y, Kim K B, Kim Y J, Lee J H, Kim Y J, and Yang S S, *Electron Mater Lett* **13** (2017) 420.
[16] 16. Gao F, Nishikawa H, Takemoto T, and Qu J M, *Microelectron Reliab* **49** (2009) 296.
[17] 17. Durst K, and Maier V, *Curr Opin Solid State Mater Sci* **19** (2015) 340.
[18] 18. Deng X, Koopman M, Chawla N, and Chawla K K, *Mater Sci Eng A* **364** (2004) 240.
[19] 19. Xiao G S, Yuan G Z, Jia C N, Yang X X, Li Z G, and Shu X F, *Mater Sci Eng A* **613** (2014) 336.
[20] 20. Xiao G S, Yang X X, Yuan G Z, Li Z G, and Shu X F, *Mater Des* **88** (2015) 520.
[21] 21. Kong X X, Zhai J J, Sun F L, Liu Y, and Zhang H, *Microelectron Reliab* **107** (2020) 113618.
[22] 22. Yahaya M Z, Ani F C, Samsudin Z, Sahin S, Abdullah M Z, and Mohamad A A, *Mater Sci Eng A* **669** (2016) 178.
[23] 23. Gao F, and Takemoto T, *Mater Lett* **60** (2006) 2315.
[24] 24. Liu C Z, and Chen J, *Mater Sci Eng A* **448** (2007) 340.
[25] 25. Shen L, Tan Z Y, and Chen Z, *Mater Sci Eng A* **561** (2013) 232.
[26] 26. Liu W S, Wang Y K, Ma Y Z, Yu Q, and Huang Y F, *Mater Sci Eng A* **653** (2016) 13.
[27] 27. Chen S W, Chen C C, Gierlotka W, Zi A R, Chen P Y and Wu H J, *J Electron Mater* **37** (2008) 992.
[28] 28. Allen W P and Perepezko J H, *Scr Met Mater* **24** (1990) 2215.
[29] 29. Allen W P and Perepezko J H, *Metall Trans A* **22** (1991) 753.
[30] Vasil'ev V P, *Russ J Phys Chem* **79** (2005) 20. Translated from *Zhurnal Fizicheskoi Khimii*, **79** (2005) 26.
[31] 31. Tunthawiroon P, and Kanlayasiri K, *T NONFERR METAL SOC* **29** (2019) 1696.
[32] 32. Xu L Y, Zhang S T, Jing H Y, and Han Y D, *J Mech Eng* **54** (2018) 2.
[33] 33. Bolshakov A, and Pharr G M, *J Mater Res* **13** (1998) 1049.
[34] 34. Cao Z H, Li P Y, and Meng X K, *Mater Sci Eng A* **516** (2009) 253.
[35] 35. Chudoba T, and Jennett N M, *J Phys D* **41** (2008) 215407.
[36] Kong X X, *Harbin University of Science and Technology* (2017).
[37] 37. Marques V M F, Wunderle B, Johnston C, and Grant P S, *Acta Mater* **61** (2013) 2471.
[38] 38. Langdon T G, *Mater Sci Eng A* **283** (2000) 266.
[39] 39. Sharma G, Ramanujan R V, Kutty T R G, and Tiwari G P, *Mater Sci Eng A* **278** (2000) 106.
[40] 40. McCabe R J, and Fine M E, *JOM* **52** (2000) 33.